Guanine nucleotide exchange factor BopE from Burkholderia pseudomallei adopts a compact version of the Salmonella SopE/SopE2 fold and undergoes a closed-to-open conformational change upon interaction with Cdc42

Abhishek Upadhyay, Huan-Lin Wu, Christopher Williams, Terry Field, Edouard E Galyov, Jean Mh van den Elsen, Stefan Bagby

Guanine nucleotide exchange factor BopE from *Burkholderia pseudomallei* adopts a compact version of the *Salmonella* SopE/SopE2 fold and undergoes a closed-to-open conformational change upon interaction with Cdc42

Abhishek UPADHYAY*†, Huan-Lin WU*†, Christopher WILLIAMS*‡, Terry FIELD§, Edouard E. GALYOV§ ‖, Jean M. H. van den ELSEN* and Stefan BAGBY*

†These authors contributed equally to this work.

*Department of Biology & Biochemistry, University of Bath, Bath BA2 7AY, UK and §Division of Environmental Microbiology, Institute for Animal Health, Compton Laboratory, Berkshire RG20 7NN, UK

‡Present address: School of Chemistry, University of Bristol, Cantock's Close, Bristol BS8 1TS, UK

‖ Present address: Department of Infection, Immunity and Inflammation, Medical Sciences Building, University of Leicester, PO Box 138, Leicester LE1 9HN, U. K.

Correspondence should be addressed to Stefan Bagby: Tel: +44 (0)1225 386436. Fax: +44 (0)1225 386779. Email: bsssb@bath.ac.uk

Running title: Structure and function of BopE

Abbreviations used: *B. mallei*, *Burkholderia mallei*; *B. pseudomallei*, *Burkholderia pseudomallei*; CPK, creatine phosphokinase; DH, Dbl homology; GEF, guanine nucleotide exchange factor; HSQC, heteronuclear single quantum coherence; IPAP, in-phase anti-phase; NMR, nuclear magnetic resonance; NOE, nuclear Overhauser effect; NOESY, nuclear Overhauser effect spectroscopy; PH, pleckstrin homology; RDC, residual dipolar coupling; rmsd, root mean square deviation; TTS, type III secretion; TTSS, type III secretion system.

BopE atomic coordinates and NMR restraints have been deposited in the Protein Data Bank (http://www.rcsb.org) under code 2JOK and 2JOL. BopE chemical shifts have been deposited in Biological Magnetic Resonance Bank (http://www.bmrb.wisc.edu; code BMRB-5974).

SYNOPSIS

BopE is a type III secreted protein from *Burkholderia pseudomallei*, the aetiological agent of melioidosis, a severe emerging infection. BopE is a guanine nucleotide exchange factor for the Rho GTPases Cdc42 and Rac1. We have determined the structure of BopE catalytic domain (amino acids 78-261) by NMR spectroscopy, showing that $BopE_{78-261}$ comprises two three-helix bundles ($\alpha1\alpha4\alpha5$ and $\alpha2\alpha3\alpha6$). This fold is similar to that adopted by BopE homologues SopE and SopE2, *Salmonella* guanine nucleotide exchange factors. Whereas the two three-helix bundles of $SopE_{78-240}$ and $SopE2_{69-240}$ form the arms of a 'A' shape, $BopE_{78-261}$ adopts a more closed conformation with substantial interactions between the two three-helix bundles. We propose that arginine and proline residues are significant in the conformational differences between BopE and SopE/E2. Analysis of the molecular interface in the $SopE_{78-240}$-Cdc42 complex crystal structure indicates that, in a BopE-Cdc42 interaction, the closed conformation of $BopE_{78-261}$ would engender steric clashes with the Cdc42 switch regions. This implies that $BopE_{78-261}$ must undergo a closed-to-open conformational change in order to catalyse guanine nucleotide exchange. In an NMR titration to investigate $BopE_{78-261}$-Cdc42 interaction, the appearance of additional peaks per NH for residues in hinge regions of $BopE_{78-261}$ indicates that $BopE_{78-261}$ does undergo a closed-to-open conformational change in the presence of Cdc42. The conformational change hypothesis is further supported by substantial improvement of $BopE_{78-261}$ catalytic efficiency through mutations that favour an open conformation. Requirement for closed-to-open conformational change explains the ten-fold to forty-fold lower k_{cat} of BopE compared to SopE and SopE2.

Key words: bacterial pathogen, guanine nucleotide exchange factor, protein-protein interaction, protein structure, Rho GTPase, type III secretion

INTRODUCTION

Burkholderia pseudomallei (*B. pseudomallei*) is the aetiological agent of melioidosis, a severe emerging infection of humans and animals that is endemic in south-east Asia and tropical Australia and that has the potential to spread worldwide [1-3]. Melioidosis has a range of clinical manifestations, including rapidly fatal septicaemia, pneumonia, skin and soft tissue abscesses, and osteomyelitis or septic arthritis. Infection is usually via contaminated soil, dust or water [4-6]. Asymptomatic infection is common in areas where the infection is endemic and progression to disease depends on the condition of the host [5]. Between the fatal and asymptomatic extremes, the infection may be chronic or run a relapsing course. Latency and relapse are common even in patients treated with appropriate antibiotics [7]. *B. pseudomallei* is closely related to *Burkholderia mallei* (*B. mallei*), the pathogen that causes glanders, a disease of horses and other solipeds. *B. mallei* can also affect humans and is often fatal if left untreated [8]. Due to the severity of the infection, aerosol infectivity and worldwide availability, both *B. pseudomallei* and *B. mallei* are considered to be potential bioweapons [9]. There is currently no vaccine against *B. pseudomallei* [10].

The molecular mechanisms of *B. pseudomallei* pathogenesis are not completely understood [11]. *B. pseudomallei* has a 7.3 Mb genome, unusually large for a prokaryote, comprising two chromosomes with sixteen genomic islands possibly acquired through very recent lateral transfer [12]. The *B. pseudomallei* genome contains at least three loci encoding putative type III secretion systems [13]. One of these, Bsa, is homologous to the inv/spa/prg type III secretion system (TTSS) of *Salmonella typhimurium* [13-15]. Type III secretion systems resemble molecular syringes for the injection of multiple bacterial effector proteins into the host cell cytoplasm that modify host cell physiology to the benefit of the pathogen [16, 17]. TTSSs are central to the virulence of many Gram negative pathogens, including *Salmonella*, *Shigella*, *Yersinia,* enteropathogenic *E. coli* and the four major genera of plant pathogenic bacteria [18, 19].

BopE, encoded within the Bsa locus, is secreted via the Bsa TTSS and influences invasion of HeLa cells probably via its function as a guanine nucleotide exchange factor (GEF) for Rho GTPases that regulate the actin network [20]. BopE shares sequence homology with the *Salmonella* translocated effector proteins SopE [21, 22] and SopE2 [23, 24] (supplemental Figure S1) which play an important role in *Salmonella* invasion of non-phagocytic intestinal epithelial cells. SopE is a potent guanine nucleotide exchange factor for the mammalian Rho GTPases Cdc42 and Rac1 *in vitro* and *in vivo* whereas SopE2 efficiently activates Cdc42 but not Rac1 [25]. The structures of SopE [26] and SopE2 [27] are entirely different from those of the best characterised eukaryotic GEFs which comprise a catalytic Dbl homology (DH) domain and an adjacent pleckstrin homology (PH) domain [28-30], although there are similarities in the catalytic mechanisms [31].

We have previously shown that BopE is monomeric in aqueous solution, adopts a single conformation that is predominantly α-helical, is stable over a wide range of pH and able to refold independently [32]. Now, as part of an examination of the structural and mechanistic relationships between BopE and its counterparts SopE and SopE2 from *Salmonella*, we report here the three-dimensional structure in solution of the catalytic domain of BopE (BopE residues 78-261 where 261 is the C-terminal residue of the full length protein) and NMR and kinetic analyses of the interaction of $BopE_{78-261}$ with the Rho GTPase Cdc42.

EXPERIMENTAL

Biophysical and biological characterisation, NMR sample generation and NMR spectroscopy of recombinant $BopE_{78-261}$

The methods used to obtain $BopE_{78-261}$ NMR samples and to derive backbone and side chain resonance assignment, plus biophysical characteristics of $BopE_{78-261}$, have been described previously [32, 33]. The ^{1}H, ^{13}C and ^{15}N chemical shifts of $BopE_{78-261}$ are in the BioMagResBank database (http://www.bmrb.wisc.edu) under accession number BMRB-5974. Biological activity of exactly the same $BopE_{78-261}$ construct as used here has been demonstrated previously: $BopE_{78-261}$ was shown to have guanine nucleotide exchange activity towards Cdc42 and Rac1 *in vitro* [20].

All NMR data were acquired at 25ºC on a Varian Unity INOVA spectrometer operating at a nominal proton frequency of 600 MHz, using a triple resonance 5 mm probe equipped with z-axis pulsed field gradients. NMR data were processed using the NMRPipe/NMRDraw software suite [34] and analysed using the SPARKY assignment program [35]. NOE distance restraints were obtained by analysis of ^{1}H-^{1}H 2D NOESY [36] (100 ms and 175 ms mixing times), ^{15}N-NOESY HSQC [37] (50 ms, 100 ms, and 150 ms mixing times) and simultaneous 3D $^{15}N/^{13}C$-edited NOESY [38] (100 ms mixing time) spectra. Backbone $^{1}D_{NH}$ residual dipolar coupling (RDC) restraints were measured for $BopE_{78-261}$ aligned with respect to the magnetic field using a stretched polyacrylamide gel; gels were made using an apparatus based on that described previously [39]. RDCs were measured using IPAP-HSQC [40].

Structure calculation

Each NOE was assigned to one of four restraint distances based on the peak intensity: 1.8-2.8 Å, 1.8-3.3 Å, 1.8-5.0 Å and 1.8-6.0 Å, corresponding to strong, medium, weak and very weak NOEs. Distances involving methyl groups, aromatic ring protons, and non-stereospecifically assigned methylene protons were represented as a $(\Sigma r^{-6})^{-1/6}$ sum [41]. 0.2 Å was added to the upper bounds for strong and medium NOE restraints involving amide

protons. Backbone dihedral angles ϕ and ψ were predicted from $^{13}C_{\alpha}$, $^{13}C_{\beta}$, $^{13}C'$, $^{1}H_{\alpha}$ and backbone ^{15}N chemical shifts using TALOS [42]. The ϕ dihedral angles were restrained to TALOS-predicted values ± 30° for α-helices and ± 40° for β-strands and ψ dihedral angles were restrained to TALOS-predicted values ± 50°. Hydrogen bond restraints were obtained from hydrogen-deuterium exchange experiments: uniformly ^{15}N-labelled $BopE_{78-261}$ in NMR buffer was lyophilised and resuspended in 99.96% D_2O. A series of ^{1}H-^{15}N HSQC spectra was then recorded to determine amide protons protected from exchange with the solvent. For hydrogen bond distance constraints, the NH-O distance was assigned lower and upper distance bounds of 1.5 and 2.5 Å, and the N-O distance assigned lower and upper distance bounds of 2.5 and 3.5 Å.

Structures were calculated using the Python interface of Xplor-NIH 2.16.0 [43, 44], using simulated annealing starting from random extended structures. Default values were used for all force constants and molecular parameters. The ensemble of NMR structures was analysed for violated restraints using the VMD-Xplor visualisation package [45]. The structure determination was carried out iteratively whereby consistently violated restraints were reassigned, wherever possible, using existing structures or removed until a consistent set of constraints was obtained with few violations in the ensemble. The ensemble of structures was further refined with Xplor-NIH standard refinement protocols using the final set of restraints. The quality of the structures was assessed using PROCHECK-NMR [46].

NMR titration of Cdc42Δ7 against $BopE_{78-261}$

Binding of unlabelled human Cdc42Δ7 to ^{15}N-labelled $BopE_{78-261}$ was monitored by recording ^{1}H-^{15}N HSQC spectra as a function of $BopE_{78-261}$:Cdc42Δ7 ratio. Cdc42Δ7 is Cdc42 lacking seven C-terminal amino acids; it was shown previously that C-terminal truncation of Cdc42 does not interfere with SopE GEF activity [47]. Cdc42Δ7 was purified from *E. coli* BL21(DE3) as previously described [47]. The NMR titration was performed as previously described [27, 48]. Briefly, two initial NMR samples were prepared in 0.5 ml NMR buffer (20 mM sodium phosphate pH 5.5, 50 mM NaCl) with 10% D_2O. Sample A contained 0.5 mM ^{15}N-labelled $BopE_{78-261}$ (molar ratio of 1.0:0.0 $BopE_{78-261}$:Cdc42Δ7) and sample B contained 0.5 mM ^{15}N-labelled $BopE_{78-261}$ and 1.34 mM Cdc42Δ7 (molar ratio of 1.0:2.7 $BopE_{78-261}$:Cdc42Δ7). The buffer composition of both samples was identical as both samples were extensively exchanged into the same batch of sample buffer. Throughout the titration the concentration of $BopE_{78-261}$ was maintained at a constant 0.5 mM and the Cdc42Δ7 concentration was varied to give a series of $BopE_{78-261}$:Cdc42Δ7 molar ratios from 1.0:0.0 to 1.0:2.7. A ^{1}H-^{15}N HSQC spectrum was acquired at each titration point with 512 complex ^{1}H points and 192 complex ^{15}N points with 32 scans per increment and spectral

widths of 8000 Hz in ^{1}H and 2000 Hz in ^{15}N. The initial NMR samples represented the end points of the titration. Intermediate values of $BopE_{78-261}$:Cdc42Δ7 were obtained by simultaneously taking equal aliquots from both sample A and sample B and then transferring the aliquots to the other NMR tube (i.e., from tube A to tube B and vice versa). This procedure was repeated until a series of twelve ^{1}H-^{15}N HSQC experiments at $BopE_{78-261}$:Cdc42Δ7 molar ratios between 1.0:0.0 and 1.0:2.7 was completed.

Generation and characterisation of BopE mutants

$BopE_{78-261}$ double mutants N224P/R230Q (mutant 1), N216P/L226P (mutant 2) and R207E/N216P (mutant 3) were made using the following pairs of primers (shown as 5'-3'): TCGCCCACGCTCGTCGAGTTCCAGCAGACGGT (N224PR230Q for) and CTGCTGGAACTCGACGAGCGTGGGCGAACGCTC (N224PR230Q rev); CGCCCGCGTTGCCGGCCGAGCGTTCGAACACGCCCGTCGAGT (N216PL226P for) and ACGGGCGTGTTCGAACGCTCGGCCGGCAACGCGGGCGCGACGA (N216PL226P rev); TGCGGAGCAGCAGGCGATCGATCTCGTCGCGCCCGCGTTGCC (R207EN216P for) and CGCGGGCGCGACGAGATCGATCGCCTGCTGCTCCGCATAC (R207EN216P rev). The mutants were constructed by overlapping PCR. The two overlapping primers (for and rev) were used in PCR with upstream and downstream primers to amplify two parts of the gene (upstream-rev and for-downstream, respectively). The resulting DNA fragments were purified, mixed and used as a template for a third PCR with upstream and downstream primers to amplify the mutated gene. The resulting DNA fragment in each case was digested with EcoR1 and BamH1 and cloned into pGEX4T1 (GE Healthcare). The cloned DNA was then sequenced. The mutant proteins were expressed and purified in the same way as wild type $BopE_{78-261}$ [32].

Filter binding assays

Cdc42Δ7 was loaded at 25ºC for 10 minutes with [^{3}H]GDP in reaction buffer containing 30 mM HEPES, 100 mM KCl, 0.1 mM EDTA, pH 7.5, 1 µg of CPK (Sigma), 0.5 mM DTT. $MgCl_2$ was added to a final concentration of 2.8 mM and the mixture was incubated for another 2 minutes. Exchange reactions were started by adding the respective guanine nucleotide exchange factor and unlabelled GDP to the reaction mixture containing Cdc42Δ7 and [^{3}H]GDP. BSA (Sigma) was used as a negative control and $SopE2_{69-240}$ was used as a positive control. Aliquots were withdrawn and the reaction stopped by quenching in ice cold wash buffer, containing 30 mM HEPES, 100 mM KCl, 0.1 mM EDTA, 5 mM $MgCl_2$, pH 7.5 followed by analysis by nitrocellulose filter binding assay [49]. Filters were washed twice with wash buffer, containing 30mM HEPES, 100 mM KCl, 0.1 mM EDTA, 5

mM $MgCl_2$, pH 7.5, dried, and radioactivity bound to the filters was analysed by scintillation counting in a Tri-Carb Liquid Scintillation Counter 1600 TR (Packard, Meriden).

RESULTS AND DISCUSSION

Structure determination of $BopE_{78-261}$

A semi-automated procedure for iterative NOE assignment was used to generate the structure of $BopE_{78-261}$. The final structures were generated using 2452 NOE-derived distance restraints (comprising 784 intra-residue, 1151 sequential and medium range and 517 long range NOEs where long range means between amino acids five or more apart in the sequence), 192 hydrogen bond restraints, 255 ϕ and ψ dihedral angle restraints (132 ϕ and 123 ψ) and 98 backbone $^1D_{NH}$ RDC restraints (Table 1). The ensemble of twenty final simulated annealing structures, selected from forty calculations on the basis of lowest energy, and the average structure are shown in Figure 1. Over the regular secondary structure elements, the ensemble of structures has a backbone rmsd from the mean of 0.65 Å and an rmsd of 1.13 Å for all non-hydrogen atoms. A Ramachandran plot of the structures with Procheck-NMR [46] indicates that 96.7% of the residues (excluding Gly and Pro residues) lie in the most favoured or additionally allowed regions. The few non-glycine residues to fall into the generously allowed regions and disallowed regions correspond to residues located at the termini or loop regions where the NMR restraint density is low.

Three-dimensional structure of $BopE_{78-261}$ and comparison with *Salmonella* $SopE_{78-240}$ and $SopE2_{69-240}$

BopE has been identified [15] as a homologue of the *Salmonella* effector proteins SopE and SopE2 (supplemental Figure S1). Overall, BopE has approximately 16% and 17% sequence identity with SopE and SopE2. Within the catalytic domain (comparing residues 78-240 of SopE and SopE2 with residues 78-240 of BopE), the sequence identity/similarity with SopE and SopE2 is approximately 25%/40% and 24%/39%.

$BopE_{78-261}$ consists of six major α-helices termed α1 to α6 arranged in two three-helix bundles, $\alpha1\alpha4\alpha5$ and $\alpha2\alpha3\alpha6$. The three-helix bundles are connected by a loop between helices α1 and α2, a β-hairpin (residues 162 to 168) followed by a loop that contains the putative (by comparison with SopE which has a ^{166}GlyAlaGlyAla^{169} catalytic motif) ^{171}GlyAlaGlyThr^{174} catalytic motif between helices α3 and α4, and a loop between helices α5 and α6 (Figure 1).

The $BopE_{78-261}$ fold is similar to that of its *Salmonella* counterparts $SopE_{78-240}$ and $SopE2_{69-240}$ but is more closed and compact with substantial interaction between the two

three-helix bundles (Figures 2 and 3). As an illustration of the more extensive association between the bundles in $BopE_{78-261}$, the buried surface areas between the three-helix bundles are 1693 $Å^2$ in $SopE_{78-240}$, 1849 $Å^2$ in $SopE2_{69-240}$ and 2148 $Å^2$ in $BopE_{78-261}$. Also, we have assigned 56 inter-bundle NOEs in $BopE_{78-261}$ compared with 20 such NOEs in our previous structure determination of $SopE2_{69-240}$ [27]. The greater conservation of bundle structure relative to bundle-bundle orientation is quantitatively illustrated by rmsd values for superimposed Cα traces and by comparison of inter-helical angles. When the catalytic domains are superimposed, the rmsd values are 2.5 Å (SopE vs SopE2), 3.9 Å (SopE2 vs BopE) and 5.0 Å (SopE vs BopE). (Note that the buried surface area and rmsd figures plus visual inspection (Figure 2) show that $SopE2_{69-240}$ is somewhat intermediate as it has a slightly more closed conformation than $SopE_{78-240}$; it must be emphasised however that the only available $SopE_{78-240}$ structure is from the complex with Cdc42 so it is possible that unbound $SopE_{78-240}$ also has a more closed $SopE2_{69-240}$–like conformation). When individual three-helix bundles are superimposed, the corresponding values are 2.3Å, 2.9Å and 2.3Å for the α1α4α5 bundle and 1.6Å, 2.8Å and 2.8Å for the α2α3α6 bundle. Calculation of inter-helical angles shows that the angles between helices in different bundles tend to differ considerably between $BopE_{78-261}$ and the two *Salmonella* GEFs (Table 2).

The interactions between the two three-helix bundles of $BopE_{78-261}$ comprise an intricate network of charge and hydrophobic interactions. Among the residues involved are five arginine residues at sequence positions 100, 182, 200, 207 and 230 that are almost unique to BopE: SopE and SopE2 do not possess arginines in any of the corresponding positions (supplemental Figure S1) but the putative bacterial GEF family member CopE from *Chromobacterium violaceum* (accession AAQ57975) has arginines corresponding to BopE Arg^{200} and Arg^{207}. Three of the BopE arginines, Arg^{200}, Arg^{207} and Arg^{230}, form part of the association between helices α5 and α6 while Arg^{182} and Glu^{125} are suitably located to link helices α4 and α2 at the putative Cdc42-binding face (based on the $SopE_{78-240}$-Cdc42 complex structure [26]) of BopE through a potential salt bridge. Arg^{100} (in helix α1) occupies a hydrophobic pocket between helices α2 and α5.

BopE residue Pro^{204} (corresponding to Ala^{199} in SopE and SopE2) promotes these inter-bundle interactions by disrupting helix α5 into two parts termed α5' and α5". As a consequence, α5' is positioned to bridge the α1α4α5 and α2α3α6 bundles and its residues are able to interact with residues in α2 and α6 of the α2α3α6 bundle (Figure 3).

In contrast to BopE Pro^{204}, three SopE/E2 prolines appear to impede inter-bundle interaction and therefore contribute to the more open conformation adopted by $SopE2_{69-240}$ in solution relative to $BopE_{78-261}$. Near to the apex of the Λ formed by the two three-helix bundles, the loop connecting α5 and α6 in $SopE2_{69-240}$ and $SopE_{78-240}$ bulges (Figure 3),

presumably due to the presence of Pro^{211}, Pro^{219} and Pro^{221}. Due to the lack of prolines at positions corresponding to 219 (Asn^{224} in BopE) and 221 (Leu^{226} in BopE), $BopE_{78-261}$ helix α6 begins earlier in the amino acid sequence than SopE/E2 α6 and the $BopE_{78-261}$ α5-α6 connecting element is a three-residue turn rather than the seven-residue loop observed in $SopE2_{69-240}$ and $SopE_{78-240}$ (Figure 3 and supplemental Figure S1). We reason that this protrusion of the polypeptide chain in the α5-α6 loop at the apex of the Λ, not observed in $BopE_{78-261}$ due to the key amino acid differences described here, counteracts extensive inter-bundle interaction in $SopE_{78-240}$ and $SopE2_{69-240}$.

NMR investigation of the interaction between $BopE_{78-261}$ and Cdc42

In order to probe $BopE_{78-261}$ binding to Cdc42 in solution, twelve 2D ^{1}H-^{15}N HQSC experiments on mixtures of varying ratios of uniformly ^{15}N-labelled $BopE_{78-261}$ and unlabelled human Cdc42Δ7 were performed. Two main types of behaviour were observed for peaks in $BopE_{78-261}$ HSQC spectra upon increasing the ratio of Cdc42Δ7 to $BopE_{78-261}$: general broadening of peaks characterised by intensity loss throughout the spectrum; and for more than one third of residues the appearance of one or more additional peaks per backbone amide NH, indicating that BopE samples more than one conformation upon interaction with Cdc42 with slow exchange between the conformations.

(A) $BopE_{78-261}$ cross peak broadening with increasing Cdc42Δ7 concentration

Almost all of the backbone NH peaks in ^{1}H-^{15}N HQSC spectra of $BopE_{78-261}$ broadened as a function of increasing Cdc42Δ7 concentration (Figure 4) until, at the highest Cdc42Δ7:$BopE_{78-261}$ ratio of 2.7:1, there was a subset of fifteen peaks that remained relatively intense (fourteen of which can be assigned as Thr^{78}, Gly^{79}, Asp^{80}, Glu^{109}, Phe^{110}, Gly^{160}, Glu^{251}, Lys^{252}, Ala^{254}, Thr^{255}, Asn^{256}, Ala^{257}, Gly^{260}, Ala^{261} and hence comprise amino acids in presumably relatively flexible parts of the protein near the N- and C-termini plus the α1-α2 and pre-β-hairpin loops) plus a subset of readily detectable peaks (some of which can be assigned as Ala^{81}, Lys^{82}, Gln^{83}, Ala^{84} (all near N-terminus), Asp^{162}, Gly^{165}, Val^{166} (β-hairpin), Gly^{190} (α4-α5 loop), Glu^{221} (α6) and Ser^{248} (unstructured C-terminal region)) and about forty further peaks that were still detectable just above the noise level. The remaining backbone NH peaks (in excess of one hundred) were broadened into the noise. Most asparagine and glutamine side chain NH_2 cross peaks were still present at the highest Cdc42Δ7:$BopE_{78-261}$ ratio of 2.7:1.0.

The rate of backbone NH peak broadening was reasonably uniform across the sequence, suggesting that the major contributors to broadening are molecular weight increase upon complexation (a 1:1 $BopE_{78-261}$:Cdc42Δ7 complex is just over double the molecular

weight of $BopE_{78-261}$), shape change upon complexation with potential for non-linear increase in effective rotational correlation time, and exchange between free and bound $BopE_{78-261}$. Due to peak overlap the degree and rate of broadening could not be quantified for a quarter of the approximately 175 backbone NH peaks. At a Cdc42Δ7:$BopE_{78-261}$ ratio of 1.0:1.0, many peaks were broadened to below 20% of their original height with the greatest concentrations of less rapidly broadened peaks found at the terminal regions, particularly the C-terminal region (Figure 4). The highest concentration of particularly rapidly broadened peaks (to noise level at a Cdc42Δ7:$BopE_{78-261}$ ratio of 1.0:1.0) occurred in helix α2; the equivalent SopE helix is involved in the interface between $SopE_{78-240}$ and Cdc42 in the $SopE_{78-240}$-Cdc42 crystal structure [26].

(B) Appearance of multiple cross peaks per $BopE_{78-261}$ backbone NH

The second major observation upon increasing the Cdc42Δ7:$BopE_{78-261}$ ratio was the appearance of a peak or peaks in addition to the original backbone NH peak for approximately seventy of the 175 backbone NH peaks; single extra peaks accounted for about 75% of these seventy cases. In fifty-six instances these additional peaks could be assigned to a particular amino acid by proximity to the corresponding original backbone NH peak. At least two of the sixteen Asn and Gln side chain NH_2 groups also displayed a second pair of peaks in the presence of Cdc42Δ7. In the vast majority of cases with one or more extra peaks, upon increasing the Cdc42Δ7:$BopE_{78-261}$ ratio the Cdc42Δ7-induced extra peaks increased in height or sometimes reached a plateau as the original backbone NH peaks decreased in height. The chemical shift difference between the original backbone NH peak and Cdc42Δ7-induced additional peak(s) at a Cdc42Δ7:$BopE_{78-261}$ ratio of 1.0:1.0 was calculated according to the formula $\Delta\delta_{ave} = [(\Delta\delta_{HN}^2 + (\Delta\delta_N^2/25))/2]^{1/2}$, where $\Delta\delta_{HN}$ and $\Delta\delta_N$ correspond to the chemical shift difference in the amide ^1H and ^{15}N chemical shifts between the original NH peak and the Cdc42Δ7-induced extra peak(s); the $\Delta\delta_{ave}$ values are shown in Figure 5A. In the cases where more than one Cdc42Δ7-induced extra peak could be assigned to a specific amino acid, the value plotted is the average of the $\Delta\delta_{ave}$ values. For sixty-seven residues, only one backbone NH peak was observed throughout the titration; the approximate sequence positions of these residues are highlighted in Figure 5A. For the remaining forty or so backbone NH peaks, overlap hindered the observation of peak behaviour during the titration.

The presence of the Cdc42Δ7-induced additional peaks for residues in several parts of $BopE_{78-261}$ indicates that $BopE_{78-261}$ samples more than one conformation in the presence of Cdc42Δ7 with the Cdc42Δ7-induced conformations in slow exchange with the initial Cdc42Δ7-free conformation. The fact that in about 75% of cases with more than one NH peak the additional peak was a single peak indicates that one Cdc42Δ7-induced conformation

was predominant. Clusters of residues exhibiting multiple backbone NH peaks are located in the α1-α2 loop and adjacent parts of α1 and α2, the β-hairpin and loops adjacent to the β-hairpin including the putative ^{171}GAGT^{174} catalytic motif, and around the α5-α6 loop (Figure 5). There is also a sequence of such residues in α6.

(C) Comparison of BopE$_{78-261}$-Cdc42 and SopE2$_{69-240}$-Cdc42 titration results

Very similar NMR titrations, both using Cdc42Δ7 and the same protocol, have now been carried out to study the BopE$_{78-261}$-Cdc42 (this work) and SopE2$_{69-240}$-Cdc42 [27] interactions. BopE$_{78-261}$ and SopE2$_{69-240}$ both experienced widespread backbone NH peak broadening upon increasing the ratio of Cdc42Δ7 to BopE$_{78-261}$/SopE2$_{69-240}$. The broadening was, if anything, more rapid in the SopE2$_{69-240}$-Cdc42Δ7 titration. The SopE2$_{69-240}$ NH peaks that underwent Cdc42Δ7-induced chemical shift changes fell into two groups, one of which showed very good agreement with the SopE$_{78-240}$ residues involved in important intermolecular interactions in the SopE$_{78-240}$-Cdc42 crystal structure [26]: this group included SopE2$_{69-240}$ residues Gln^{109} (α2), Asp^{124} (α2), Gly^{165} (adjacent to catalytic motif), Gly^{166}, Gly^{168}, Ala^{169} (all catalytic motif), Val^{174} (α4), Gln^{194} (α5) and Lys^{198} (α5). The second group of perturbed SopE2$_{69-240}$ residues comprised several scattered internal residues and isolated residues on the opposite side of the molecule to the binding interface. In contrast to SopE2$_{69-240}$, slow exchange between unbound and Cdc42Δ7–bound conformations of BopE$_{78-261}$ was observed during the BopE$_{78-261}$-Cdc42Δ7 titration. The chemical shift differences between these states of BopE$_{78-261}$ were, in general, four to five or more times the magnitude of the Cdc42Δ7–induced chemical shift changes observed in the SopE2$_{69-240}$-Cdc42Δ7 titration. The BopE equivalents (BopE residues Asp^{128}, Gly^{171}, Gly^{173}, Thr^{174} and Thr^{179}) of five of the Cdc42-perturbed SopE2$_{69-240}$ residues (SopE2$_{69-240}$ residues Asp^{124}, Gly^{166}, Gly^{168}, Ala^{169} and Val^{174}) listed above were involved in the Cdc42-induced slow conformational exchange whereas Ser^{170}, Tyr^{199} and Gln^{203}, the BopE equivalents of SopE residues Gly^{165}, Gln^{194} and Lys^{198}, were not. The behaviour of Gln^{113} (BopE equivalent of SopE Gln^{109}) during the titration could not be monitored due to peak overlap. Of the BopE equivalents of a further two SopE$_{78-240}$ residues that interact with Cdc42 in the SopE$_{78-240}$-Cdc42 crystal structure but that were not significantly perturbed in the SopE2$_{69-240}$-Cdc42Δ7 NMR titration [27], Ala^{135} (α2-α3 loop) was involved in the Cdc42-induced slow conformational exchange but the behaviour of Asp^{107} could not be monitored due to peak overlap. The significance of the positions of slowly exchanging residues in BopE$_{78-261}$ is discussed in the next section.

Implications of $BopE_{78-261}$ tertiary structure and $BopE_{78-261}$-Cdc42 NMR titration for BopE interaction with Rho GTPases

The question arises as to whether the conformational difference between the catalytic domain of BopE and those of SopE and SopE2 has implications for interaction with Rho GTPases. Analysis of the interface between $SopE_{78-240}$ and Cdc42 in the $SopE_{78-240}$–Cdc42 complex crystal structure [26] reveals that the interaction can be broken down into two major components: a groove on $SopE_{78-240}$ accommodates a ridge on Cdc42 formed by residues 35 to 41 (switch region I) and the gap between the two three-helix bundles of $SopE_{78-240}$ accommodates Cdc42 residues Val^{36} and Asp^{38} (supplemental Figure 2). The latter interaction in particular indicates that, in its closed conformation, $BopE_{78-261}$ would experience steric clashes with Cdc42. The resulting implication is that BopE catalytic domain must undergo a change from its closed conformation to a more open conformation like those of SopE and SopE2 catalytic domains in order to carry out its guanine nucleotide exchange function. A requirement for such a large scale conformational change is consistent with, and may at least partially explain, the observed differences in turnover number for guanine nucleotide exchange between $BopE_{78-261}$ and its *Salmonella* counterparts: a k_{cat} of 0.48 s^{-1} was measured for $BopE_{78-261}$–induced guanine nucleotide exchange in Rac1 (a similar rate was measured for Cdc42) [20], whereas the k_{cat} values for guanine nucleotide exchange in Cdc42 are 5 ± 1 s^{-1} and 19 ± 3 s^{-1} for $SopE_{78-240}$ and $SopE2_{69-240}$ respectively [25].

It might then be asked whether BopE catalytic domain exists in equilibrium in solution between closed and open forms, or does it undergo a conformational change upon interaction with target protein? These two possibilities are not necessarily mutually exclusive – there may be an equilibrium in solution for unbound BopE catalytic domain but one that lies strongly towards the closed conformation. The results of the $BopE_{78-261}$-Cdc42Δ7 titration are consistent with a significant conformational change in $BopE_{78-261}$ upon binding to Cdc42: when superimposed on the structure of $BopE_{78-261}$ (Figure 5B), it is apparent that many of the amino acids that sampled one or more Cdc42Δ7-induced conformations during the $BopE_{78-261}$-Cdc42Δ7 titration are located in potential hinge areas for a closed-to-open conformational change involving relative reorientation of the two three-helix bundles of $BopE_{78-261}$. These hinge areas include the α1-α2 loop and adjacent residues in α1 and α2, residues in the region between α3 and α4 that includes the β-hairpin and ^{171}GAGT^{174} putative catalytic motif, and residues in and around the α5-α6 turn. Residues in the central part of α2 also show slow exchange between initial and Cdc42Δ7-induced conformations, consistent with a change in conformation and/or position of the α3-α4 loop C-terminal to the β-hairpin that associates with this part of α2 in Cdc42-free $BopE_{78-261}$ (Figure 1). It is also striking that few of the amino acids with multiple NH peaks are located in areas that would be involved in any intra-

bundle conformational changes, suggesting that the three-helix bundles themselves remain largely unchanged. The considerably greater magnitude of the Cdc42Δ7–induced chemical shift differences between free and Cdc42Δ7-bound states of $BopE_{78-261}$ compared to the magnitude of the chemical shift changes observed in the $SopE2_{69-240}$-Cdc42Δ7 titration underpin the conclusion that $BopE_{78-261}$ undergoes greater structural change than $SopE2_{69-240}$ upon binding of the Rho GTPase.

Guanine nucleotide exchange activity of $BopE_{78-261}$ and $BopE_{78-261}$ mutants

In order to investigate further the requirement for a conformational change in BopE for catalysis of nucleotide exchange in Rho GTPases, three $BopE_{78-261}$ double mutants were made. These were N224P/R230Q (mutant 1), N216P/L226P (mutant 2) and R207E/N216P (mutant 3). The mutations were selected according to their potential for changing $BopE_{78-261}$ from its relatively closed conformation to a more open conformation closer to those observed for $SopE_{78-240}$ in its complex with Cdc42 [26] and unbound $SopE2_{69-240}$ [27], as follows: N224P to induce a SopE/E2-like bulge in the α5-α6 loop; R230Q to further disrupt the α5-α6 interaction; N216P and L226P to induce a SopE/E2-like bulge in the α5-α6 loop; R207E to disrupt the α5-α6 interaction and N216P to induce a SopE/E2-like bulge in the α5-α6 loop.

Like the wild type recombinant $BopE_{78-261}$, the mutants were cloned and expressed as GST fusions. Mutant 1 expressed relatively poorly in *E. coli* but could be purified, mutant 2 expressed at low levels but disappeared during purification (perhaps this mutant is misfolded and therefore rapidly degraded) and mutant 3 expressed well and could be purified. In filter binding assays [49] with bovine serum albumin as negative control, the order of nucleotide exchange catalytic efficiency was: $BopE_{78-261}$ N224P/R230Q (mutant 1) > $SopE2_{69-240}$ > wild type $BopE_{78-261}$ >> $BopE_{78-261}$ R207E/N216P (mutant 3); in fact, mutant 3 showed essentially no catalytic activity (Figure 6). The reason for the lack of nucleotide exchange activity in mutant 3 is unclear but the R207E/N216P double mutation obviously induces changes that disrupt rather than enhance BopE function. The N224P/R230Q double mutation in $BopE_{78-261}$, on the other hand, produces a much more effective guanine nucleotide exchange factor than wild type $BopE_{78-261}$ and a better guanine nucleotide exchange factor than even $SopE2_{69-240}$ (Figure 6), itself a better guanine nucleotide exchange factor for Cdc42 than $SopE_{78-240}$ [25]. This result, showing that mutations designed to abrogate important inter-bundle interactions and thereby induce a more open conformation in $BopE_{78-261}$ can substantially improve nucleotide exchange catalytic efficiency, adds further strong experimental support to that from NMR titration for the hypothesis that BopE GEF domain undergoes Rho GTPase-induced change from a closed to an open conformation.

CONCLUSIONS

The molecular mechanisms of *B. pseudomallei* pathogenesis are not well understood. A number of putative type III-secreted effector proteins have been identified by analysis of the *B. pseudomallei* genome sequence [15]. One of these proteins, BopE, is a homologue of the potent guanine nucleotide exchange factors SopE [21, 50] and SopE2 [23, 24] from *Salmonella enterica* (supplemental Figure S1). SopE and SopE2 catalyse nucleotide exchange in mammalian Rho GTPases, contributing to disruption of the host cell membrane and invasion of the host cell [17, 21, 23, 25, 50, 51]. BopE likewise acts as a GEF for the Rho GTPases Cdc42 and Rac1 *in vitro* and may play a role in the invasion of non-phagocytic epithelial cells [20]. This work shows that BopE and SopE/SopE2 catalytic domains adopt similar three-dimensional folds comprising two three-helix bundles but also shows that BopE has a more compact conformation, involving significant inter-bundle interaction, than its *Salmonella* homologues. The most open conformation of the three is for Cdc42-bound $SopE_{78\text{-}240}$, with unbound $SopE2_{69\text{-}240}$ slightly more closed. It is worth noting, however, that SopE residues involved in contacting Cdc42 in the $SopE_{78\text{-}240}$-Cdc42 complex crystal structure [26] are largely conserved or conservatively substituted in BopE (supplemental Figure S1). SopE residues (Asp^{103}, Gln^{109}, Asp^{124} and Gly^{168}) shown by mutation to be functionally important [31] are, moreover, conserved in BopE. It seems likely, therefore, that despite its more closed conformation, BopE ultimately utilises the same mechanism as SopE and other Rho GEFs [52] in catalysing guanine nucleotide exchange in Rho GTPases. This would require that BopE change from closed to open conformations in the presence of Rho GTPase target proteins. Such a conformational change is evidenced here by the results of a $BopE_{78\text{-}261}$-Cdc42 NMR titration and measurements of nucleotide exchange catalytic efficiency comparing wild type and mutant BopE GEF domain. Phosphorylation of BopE would not seem to be required for any conformational change as we and others have shown that $BopE_{78\text{-}261}$ purified from *E. coli* exhibits guanine nucleotide exchange factor activity [20]. Finally, given the sequence and conformational differences between BopE and SopE/E2 catalytic domains, it is possible that there are as yet unknown differences in specificity among the members of this family of bacterial guanine nucleotide exchange factors, with the potential for modulation of the activities of small G-proteins in addition to Cdc42 and Rac1.

ACKNOWLEDGEMENTS

This work was supported at Bath by The Wellcome Trust (grant 060998) and at IAH by BBSRC. The Wellcome Trust is acknowledged for purchase of the 600 MHz NMR spectrometer (grant 051902) used in this study. C.W. was supported by a PhD studentship from EPSRC. We thank Julian Eaton (Bath) for constructive criticism of the manuscript and help with rmsd calculations, Lewis Kay (Toronto) for some of the pulse sequences used here, Charles Schwieters for help with the Python interface of Xplor-NIH, Kyoko Yap for the programme Interhlx, Graham Pavitt's group (Manchester) for instruction on filter binding assays and Mareike Posner (Bath) for advice on enzyme assays.

REFERENCES

1 Dance, D. A. B. (2002) Melioidosis. Curr. Opin. Infect. Dis. **15**, 127-132

2 White, N. J. (2003) Melioidosis. Lancet **361**, 1715-1722

3 Peacock, S. J. (2006) Melioidosis. Curr. Opin. Infect. Dis. **19**, 421-428

4 Brett, P. J. and Woods, D. E. (2000) Pathogenesis of and immunity to melioidosis. Acta Tropica **74**, 201-210

5 Currie, B. J., Fisher, D. A., Howard, D. M., Burrow, J. N. C., Lo, D., Selva-Nayagam, S., Anstey, N. M., Huffam, S. E., Snelling, P. L., Marks, P. J., Stephens, D. P., Lum, G. D., Jacups, S. P. and Krause, V. L. (2000) Endemic melioidosis in tropical northern Australia: a 10-year prospective study and review of the literature. Clin. Infect. Dis. **31**, 981-986

6 Currie, B. J., Fisher, D. A., Anstey, N. M. and Jacups, S. P. (2000) Melioidosis: acute and chronic disease, relapse and re- activation. Trans. Roy. Soc. Trop. Med. Hygiene **94**, 301-304

7 Chaowagul, W., Suputtamongkol, Y., Dance, D. A. B., Rajchanuvong, A., Pattaraarechachai, J. and White, N. J. (1993) Relapse in melioidosis - incidence and risk factors. J. Infect. Dis. **168**, 1181-1185

8 Wilkinson, L. (1981) Glanders: medicine and veterinary medicine in common pursuit of a contagious disease. Med. Hist. **25**, 363-384

9 Rotz, L., Khan, A., Lillibridge, S., Ostroff, S. and Hughes, J. (2002) Public health assessment of potential biological terrorism agents. Emerg. Infect. Dis. **8**, 225-230

10 Haque, A., Chu, K., Easton, A., Stevens, M. P., Galyov, E. E., Atkins, T., Titball, R. and Bancroft, G. J. (2006) A live experimental vaccine against *Burkholderia pseudomallei* elicits CD4(+) T cell-mediated immunity, priming T cells specific for 2 type III secretion system proteins. J. Infect. Dis. **194**, 1241-1248

11 Stevens, M. P. and Galyov, E. E. (2004) Exploitation of host cells by *Burkholderia pseudomallei*. Intl. J. Med. Microbiol. **293**, 549-555

12 Holden, M. T. G., Titball, R. W., Peacock, S. J., Cerdeno-Tarraga, A. M., Atkins, T., Crossman, L. C., Pitt, T., Churcher, C., Mungall, K., Bentley, S. D., Sebaihia, M., Thomson, N. R., Bason, N., Beacham, I. R., Brooks, K., Brown, K. A., Brown, N. F., Challis, G. L., Cherevach, I., Chillingworth, T., Cronin, A., Crossett, B., Davis, P., DeShazer, D., Feltwell, T., Fraser, A., Hance, Z., Hauser, H., Holroyd, S., Jagels, K., Keith, K. E., Maddison, M., Moule, S., Price, C., Quail, M. A., Rabbinowitsch, E., Rutherford, K., Sanders, M., Simmonds, M., Songsivilai, S., Stevens, K., Tumapa, S., Vesaratchavest, M., Whitehead, S., Yeats, C., Barrell, B. G., Oyston, P. C. F. and Parkhill, J. (2004) Genornic plasticity of the causative agent of melioidosis, *Burkholderia pseudomallei*. Proc. Natl. Acad. Sci. U.S.A. **101**, 14240-14245

13 Rainbow, L., Hart, C. A. and Winstanley, G. (2002) Distribution of type III secretion gene clusters in *Burkholderia pseudomallei*, *B. thailandensis* and *B. mallei*. J. Med. Microbiol. **51**, 374-384

14 Attree, O. and Attree, I. (2001) A second type III secretion system in *Burkholderia pseudomallei*: Who is the real culprit? Microbiol. **147**, 3197-3199

15 Stevens, M. P., Wood, M. W., Taylor, L. A., Monaghan, P., Hawes, P., Jones, P. W., Wallis, T. S. and Galyov, E. E. (2002) An inv/mxi-spa-like type III protein secretion system in *Burkholderia pseudomallei* modulates intracellular behaviour of the pathogen. Mol. Microbiol. **46**, 649-659

16 Johnson, S., Deane, J. E. and Lea, S. M. (2005) The type III needle and the damage done. Curr. Opin. Struct. Biol. **15**, 700-707

17 Galàn, J. E. and Wolf-Watz, H. (2006) Protein delivery into eukaryotic cells by type III secretion machines. Nature **444**, 567-573

18 Cornelis, G. R. and Van Gijsegem, F. (2000) Assembly and function of type III secretory systems. Ann. Rev. Microbiol. **54**, 735-774

19 Pallen, M. J., Beatson, S. A. and Bailey, C. M. (2005) Bioinformatics, genomics and evolution of non-flagellar type-III secretion systems: a Darwinian perpective. FEMS Microbiol. Rev. **29**, 201-229

20 Stevens, M. P., Friebel, A., Taylor, L. A., Wood, M. W., Brown, P. J., Hardt, W.-D. and Galyov, E. E. (2003) A *Burkholderia pseudomallei* type III secreted protein, BopE, facilitates bacterial invasion of epithelial cells and exhibits guanine nucleotide exchange factor activity. J. Bact. **185**, 4992-4996

21 Wood, M. W., Rosqvist, R., Mullan, P. B., Edwards, M. H. and Galyov, E. E. (1996) SopE, a secreted protein of *Salmonella dublin*, is translocated into the target eukaryotic cell via a Sip-dependent mechanism and promotes bacterial entry. Mol. Microbiol. **22**, 327-338

22 Hardt, W. D., Chen, L. M., Schuebel, K. E., Bustelo, X. R. and Galàn, J. E. (1998) *S. typhimurium* encodes an activator of Rho GTPases that induces membrane ruffling and nuclear responses in host cells. Cell **93**, 815-826

23 Bakshi, C. S., Singh, V. P., Wood, M. W., Jones, P. W., Wallis, T. S. and Galyov, E. E. (2000) Identification of SopE2, a *Salmonella* secreted protein which is highly homologous to SopE and involved in bacterial invasion of epithelial cells. J. Bact. **182**, 2341-2344

24 Stender, S., Friebel, A., Linder, S., Rohde, M., Mirold, S. and Hardt, W. D. (2000) Identification of SopE2 from *Salmonella typhimurium*, a conserved guanine nucleotide exchange factor for cdc42 of the host cell. Mol. Microbiol. **36**, 1206-1221

25 Friebel, A., Ilchmann, H., Aelpfelbacher, M., Ehrbar, K., Machleidt, W. and Hardt, W. D. (2001) SopE and SopE2 from *Salmonella typhimurium* activate different sets of Rho GTPases of the host cell. J. Biol. Chem. **276**, 34035-34040

26 Buchwald, G., Friebel, A., Galàn, J. E., Hardt, W. D., Wittinghofer, A. and Scheffzek, K. (2002) Structural basis for the reversible activation of a Rho protein by the bacterial toxin SopE. EMBO J. **21**, 3286-3295

27 Williams, C., Galyov, E. E. and Bagby, S. (2004) Solution structure, backbone dynamics, and interaction with Cdc42 of *Salmonella* guanine nucleotide exchange factor SopE2. Biochemistry **43**, 11998-12008

28 Cerione, R. A. and Zheng, Y. (1996) The Dbl family of oncogenes. Curr. Opin. Cell Biol. **8**, 216-222

29 Snyder, J. T., Worthylake, D. K., Rossman, K. L., Betts, L., Pruitt, W. M., Siderovski, D. P., Der, C. J. and Sondek, J. (2002) Structural basis for the selective activation of Rho GTPases by Dbl exchange factors. Nat. Struct. Biol. **9**, 468-475

30 Rehmann, H., Wittinghofer, A. and Bos, J. L. (2007) Capturing cyclic nucleotides in action: snapshots from crystallographic studies. Nat. Rev. Mol. Cell Biol. **8**, 63-73

31 Schlumberger, M. C., Friebel, A., Buchwald, G., Scheffzek, K., Wittinghofer, A. and Hardt, W.-D. (2003) Amino acids of the bacterial toxin SopE involved in G nucleotide exchange on Cdc42. J. Biol. Chem. **278**, 27149-27159

32 Upadhyay, A., Williams, C., Gill, A. C., Philippe, D. L., Davis, K., Taylor, L. A., Stevens, M. P., Galyov, E. E. and Bagby, S. (2004) Biophysical characterization of the catalytic domain of guanine nucleotide exchange factor BopE from *Burkholderia pseudomallei*. Biochim. Biophys. Acta **1698**, 111-119

33 Wu, H.-L., Williams, C., Upadhyay, A., Galyov, E. E. and Bagby, S. (2004) Assignment of the ^{1}H, ^{13}C and ^{15}N resonances of the catalytic domain of guanine nucleotide exchange factor BopE from *Burkholderia pseudomallei*. J. Biomol. NMR **29**, 215-216

34 Delaglio, F., Grzesiek, S., Vuister, G. W., Zhu, G., Pfeifer, J. and Bax, A. (1995) NMRPipe: a multidimensional spectral processing system based on Unix pipes. J. Biomol. NMR **6**, 277-293

35 Goddard, T. D. and Kneller, D. G. Sparky 3. University of California, San Francisco

36 Macura, S. and Ernst, R. R. (1980) Elucidation of cross-relaxation in liquids by two-dimensional NMR spectroscopy. J. Phys. **41**, 95-117

37 Zhang, O. W., Kay, L. E., Olivier, J. P. and Forman-Kay, J. D. (1994) Backbone ^{1}H and ^{15}N resonance assignments of the N-terminal SH3 domain of drk in folded and unfolded states using enhanced-sensitivity pulsed-field gradient NMR techniques. J. Biomol. NMR **4**, 845-858

38 Pascal, S. M., Muhandiram, D. R., Yamazaki, T., Forman-Kay, J. D. and Kay, L. E. (1994) Simultaneous acquisition of ^{15}N-edited and ^{13}C-edited NOE spectra of proteins dissolved in H_2O. J. Magn. Reson. Ser. B **103**, 197-201

39 Chou, J. J., Gaemers, S., Howder, B., Louis, J. M. and Bax, A. (2001) A simple apparatus for generating stretched polyacrylamide gels, yielding uniform alignment of proteins and detergent micelles. J. Biomol. NMR**21**, 377-382

40 Ottiger, M., Delaglio, F. and Bax, A. (1998) Measurement of J and dipolar couplings from simplified two-dimensional NMR spectra. J. Magn. Reson. **131**, 373-378

41 Nilges, M. (1993) A calculation strategy for the structure determination of symmetrical dimers by ^{1}H NMR. Proteins-Struct. Funct. Genet. **17**, 297-309

42 Cornilescu, G., Delaglio, F. and Bax, A. (1999) Protein backbone angle restraints from searching a database for chemical shift and sequence homology. J. Biomol. NMR **13**, 289-302

43 Schwieters, C. D., Kuszewski, J. J., Tjandra, N. and Clore, G. M. (2003) The Xplor-NIH NMR molecular structure determination package. J. Magn. Reson. **160**, 65-73

44 Schwieters, C. D., Kuszewski, J. J. and Clore, G. M. (2006) Using Xplor-NIH for NMR molecular structure determination. Prog. Nuc. Magn. Res. Spect. **48**, 47-62

45 Schwieters, C. D. and Clore, G. M. (2001) The VMD-Xplor visualization package for NMR structure refinement. J. Magn. Reson. **149**, 239-244

46 Laskowski, R. A., Rullmann, J. A. C., MacArthur, M. W., Kaptein, R. and Thornton, J. M. (1996) Aqua and Procheck-NMR: programs for checking the quality of protein structures solved by NMR. J. Biomol. NMR **8**, 477-486

47 Rudolph, M. G., Weise, C., Mirold, S., Hillenbrand, B., Bader, B., Wittinghofer, A. and Hardt, W. D. (1999) Biochemical analysis of SopE from *Salmonella typhimurium*, a highly efficient guanosine nucleotide exchange factor for Rho GTPases. J. Biol. Chem. **274**, 30501-30509

48 McAlister, M. S. B., Mott, H. R., van der Merwe, P. A., Campbell, I. D., Davis, S. J. and Driscoll, P. C. (1996) NMR analysis of interacting soluble forms of the cell-cell recognition molecules CD2 and CD48. Biochemistry **35**, 5982-5991

49 Self, A. J. and Hall, A. (1995) Measurement of intrinsic nucleotide exchange and GTP hydrolysis rates. Meth. Enzymol. **256**, 67-76

50 Hardt, W. D., Chen, L. M., Schuebel, K. E., Bustelo, X. R. and Galàn, J. E. (1998) *S. Typhimurium* encodes an activator of Rho GTPases that induces membrane ruffling and nuclear responses in host cells. Cell **93**, 815-826

51 Friebel, A. and Hardt, W. D. (2000) Purification and biochemical activity of *Salmonella* exchange factor SopE. Meth. Enzymol. **325**, 82-91

52 Thomas, C., Fricke, I., Scrima, A., Berken, A. and Wittinghofer, A. (2007) Structural evidence for a common intermediate in small G protein-GEF reactions. Mol. Cell **25**, 141-149

Table 1 Structural statistics on NMR-derived structures of BopE GEF domain

Total number of NOE restraints	2452
intraresidue	784
sequential/med. range (*i* to *i*+1—4)	1151
long range	517
Number of dihedral angle restraints	255
Number of hydrogen bond restraints	192
Number of backbone $^{1}D_{NH}$ RDC restraints	98
Rmsd for backbone atoms[a]	0.65Å
Rmsd for non-hydrogen atoms[a]	1.15Å
Average numbers of NOE violations	
>0.3Å (per structure)	5
>0.5Å (per structure)	1
Average number of dihedral angle violations	
>5° (per structure)	0

	Average structure	Ensemble
Ramachandran plot regions[b]		
Most favoured (%)	88.8	80.8
Additional allowed (%)	8.7	15.9
Generously allowed (%)	1.9	2.6
Disallowed (%)	0.6	0.7

[a]The rmsd from the mean structure calculated over residues 83-99, 110-133, 143-156, 177-189, 205-217, and 220-246. [b]Calculated with PROCHECK-NMR [46].

Table 2 Comparison of helix crossing angles in the solution structures of $BopE_{78-261}$ and $SopE_{69-240}$ and the crystal structure of Cdc42-bound $SopE_{78-240}$

	Crossing angle (deg)[a]					
helix pair	$BopE_{78-261}$	$SopE2_{69-240}$[b]	$SopE_{78-240}$[c]	Δ1[d]	Δ2[e]	Δ3[f]
1-2	155.68	144.63	140.08	11.05	15.60	4.55
1-3	-35.28	-39.37	-44.45	4.09	9.17	5.08
1-4	137.08	131.03	132.95	6.05	4.13	-1.92
1-5	-21.02	-37.61	-34.47	16.59	13.45	3.14
1-6	152.68	133.14	126.04	19.54	26.64	7.10
2-3	167.18	159.41	165.24	7.77	1.94	-5.83
2-4	-49.60	-77.02	-79.58	27.42	29.98	2.56
2-5	-158.43	-134.98	-133.83	-23.45	-24.60	-1.15
2-6	-3.46	-16.15	-14.14	12.69	10.68	-2.01
3-4	131.60	114.21	105.35	17.39	26.25	8.86
3-5	-24.31	28.47	37.81	-52.78	-62.12	-9.34
3-6	170.61	166.69	163.04	3.92	7.57	3.65
4-5	151.66	141.47	142.39	10.19	9.27	-0.92
4-6	-49.40	-78.97	-90.72	29.57	41.32	11.75
5-6	157.99	138.28	125.41	19.71	32.58	12.87

[a]Calculated with Interhlx (K. Yap, University of Toronto; (http://nmr.uhnres.utoronto.ca/ikura/interhlx). [b]SopE2 GEF domain NMR structure (PDB entry 1R9K). [c]SopE GEF domain crystal structure (PDB entry 1GZS). [d]The $BopE_{78-261}$ helix crossing angle minus the $SopE2_{69-240}$ helix crossing angle. [e]The $BopE_{78-261}$ helix crossing angle minus the $SopE_{78-240}$ helix crossing angle. [f]The $SopE2_{69-240}$ helix crossing angle minus the $SopE_{78-240}$ helix crossing angle.

FIGURE LEGENDS

Figure 1 Structure of the BopE GEF domain (residues 78-261)

(A) Backbone (N, C^{α} and C') trace of the twenty lowest energy structures coloured as a continuum from blue at N-terminus to red at C-terminus.

(B) Ribbon diagram of the average structure coloured as in part A. The α-helices and β-hairpin are labelled. The ^{171}GAGT^{174} putative catalytic motif lies between the β-hairpin and α4.

Figure 2 Comparison of the structures of SopE, SopE2 and BopE catalytic GEF domains Representations of the crystal structure of Cdc42-bound $SopE_{78-240}$ (green; PDB code 1GZS), solution structure of $SopE2_{69-240}$ (cyan; PDB codes 1R6E and 1R9K) and solution structure of $BopE_{78-261}$ (purple; PDB codes 2JOK and 2JOL) demonstrating the similarities and differences in the $SopE_{78-240}$, $SopE2_{69-240}$ and $BopE_{78-261}$ structures. All three structures consist of two three-helix bundles with a connecting β-hairpin that is followed by a loop that contains the ^{166}GAGA^{169} (SopE/E2) / ^{171}GAGT^{174} (BopE) catalytic motif.

Figure 3 $SopE_{78-240}$ and $BopE_{78-261}$ conformation comparison

In order to highlight the major secondary structure and conformational differences between $SopE_{78-240}$ (green) and $BopE_{78-261}$ (purple), the α-helices of the two structures are shown and the locations of relevant proline residues are highlighted. Note the contrast between the protuberance of the α5-α6 loop in $SopE_{78-240}$ due to Pro^{211}, Pro^{219} and Pro^{221} and the compactness of the corresponding turn in $BopE_{78-261}$. Also note the disruption of $BopE_{78-261}$ helix α5 by Pro^{204} into two parts, labelled α5' and α5", that permits α5' in particular to interact with the α2α3α6 bundle. Both characteristics arise from the presence or absence of proline residues and result in the greater compactness of $BopE_{78-261}$ relative to $SopE_{78-240}$ and $SopE2_{69-240}$. The viewpoint for this figure is approximately 180º different from that used for Figures 1 and 2.

Figure 4 Reduction in $BopE_{78-261}$ backbone NH peak height as a function of BopE residue number upon titration with Cdc42Δ7

The percentage reduction in peak height is shown at a $BopE_{78-261}$:Cdc42Δ7 molar ratio of 1.0:1.0. Only one $BopE_{78-261}$ residue, Cys-131, showed no reduction in peak

height. For the remainder of residues that appear with 0% reduction on this plot, peak height could not be quantified due to peak overlap. Note that prolines, which do not give rise to peaks in ^{1}H-^{15}N HSQC spectra and so are not monitored in this titration, occur at $BopE_{78-261}$ sequence positions 102, 134, 143, 159, 169, 176, 197, 204 and 219.

Figure 5 $BopE_{78-261}$ residues that show slow conformational exchange in the presence of Cdc42Δ7

(A) Average chemical shift differences plotted as a function of BopE residue number. The values were calculated using $\Delta\delta_{ave} = [(\Delta\delta_{HN}^{2} + (\Delta\delta_{N}^{2}/25))/2]^{1/2}$, where $\Delta\delta_{HN}$ and $\Delta\delta_{N}$ correspond to the chemical shift difference in the amide proton and ^{15}N chemical shifts between the original NH peak and the Cdc42Δ7-induced extra peak(s). The approximate sequence positions of the sixty-seven residues for which only one backbone NH peak was observed are indicated by asterisks.

(B) The average structure of $BopE_{78-261}$. Amino acids for which one or more additional backbone NH peaks appeared in $BopE_{78-261}$ ^{1}H-^{15}N HSQC spectra during the $BopE_{78-261}$-Cdc42Δ7 titration are shown in yellow, the remainder are shown in purple.

Figure 6 Kinetic analysis by filter binding assay of guanine nucleotide exchange in Cdc42 mediated by $BopE_{78-261}$, $BopE_{78-261}$ mutants and $SopE2_{69-240}$

Radioactivity was measured as counts per minute (CPM). Log of CPM was plotted against time and the gradient of a best-fit line was taken as a measure of guanine nucleotide exchange efficiency (rate of change in radioactivity as a function of time). The catalytic efficiency rank is: $BopE_{78-261}$ N224P/R230Q (mutant 1; gradient -0.5831) > $SopE2_{69-240}$ (gradient -0.5038) > wild type $BopE_{78-261}$ (gradient -0.3658) >> $BopE_{78-261}$ R207E/N216P (mutant 3) and BSA (both gradient 0.0038). $BopE_{78-261}$ N224P/R230Q (mutant 1) is therefore a better catalyst of guanine nucleotide exchange in Cdc42 than $SopE2_{69-240}$ and a much better catalyst than wild type $BopE_{78-261}$.

Figure 1

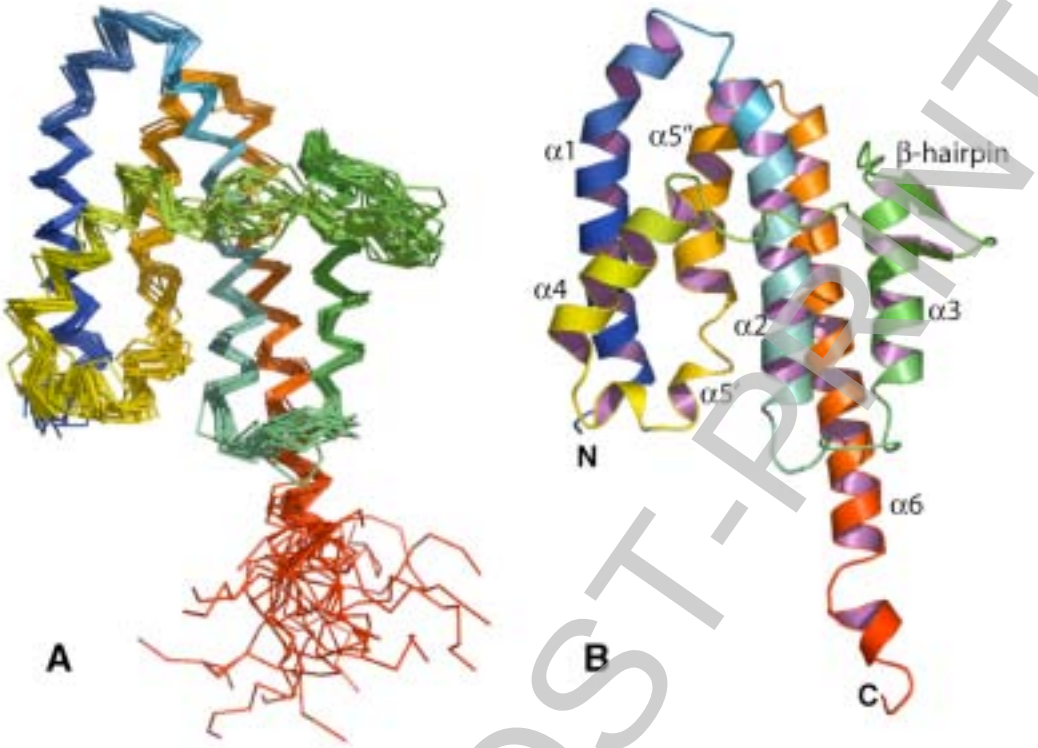

Figure 2

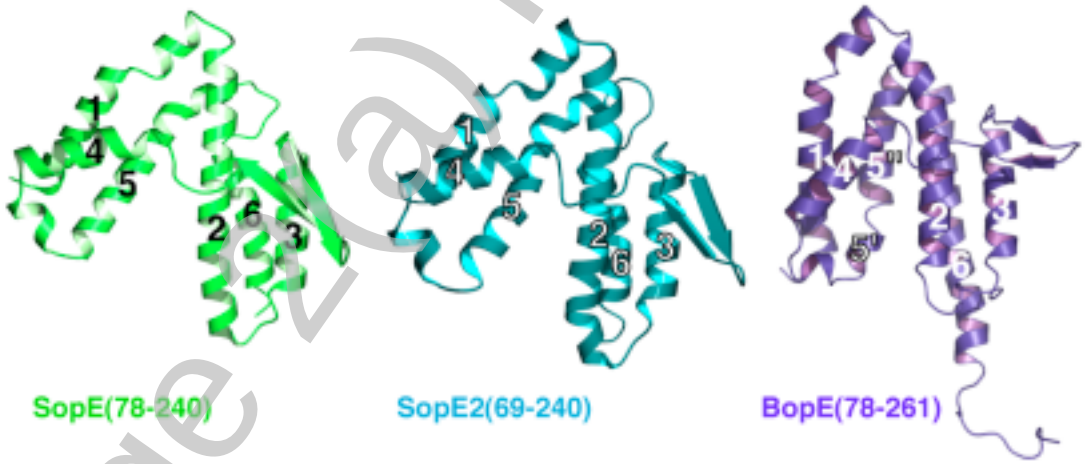

Figure 3

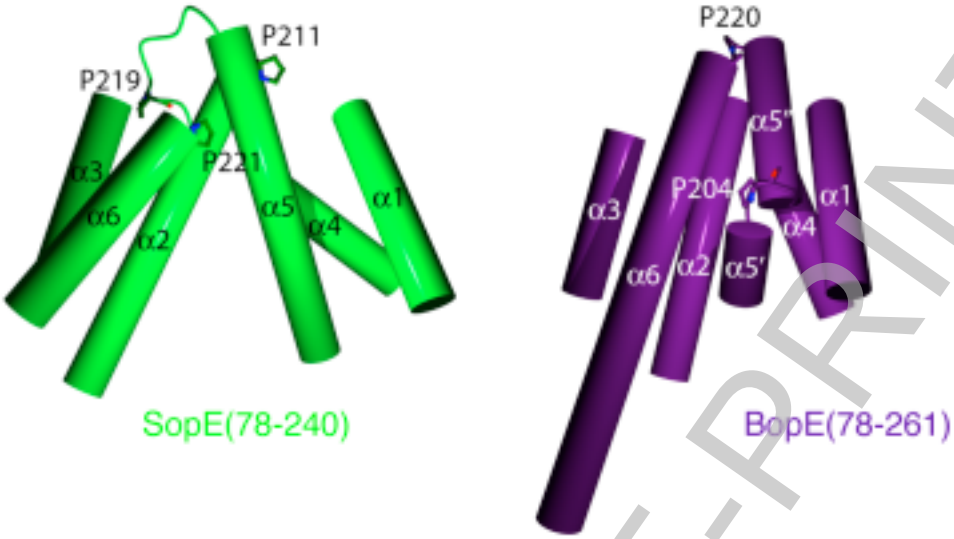

Figure 4

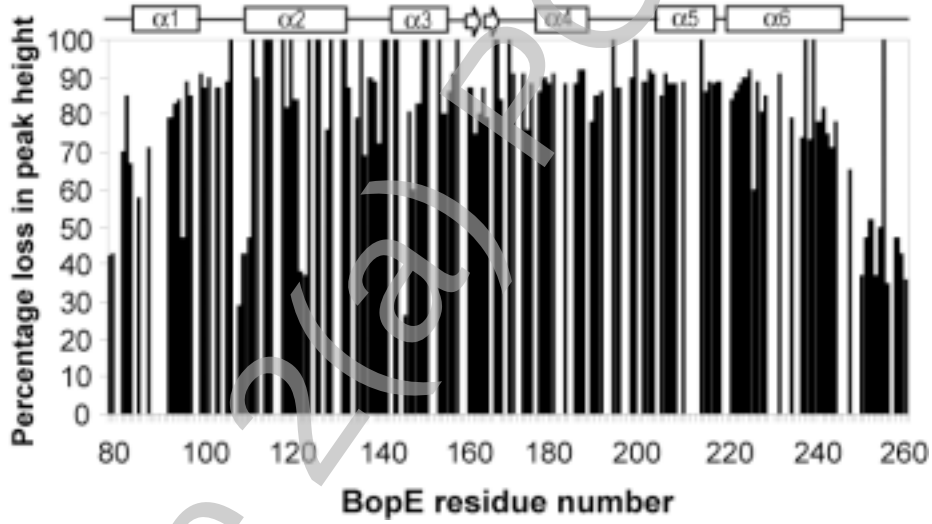

Figure 5

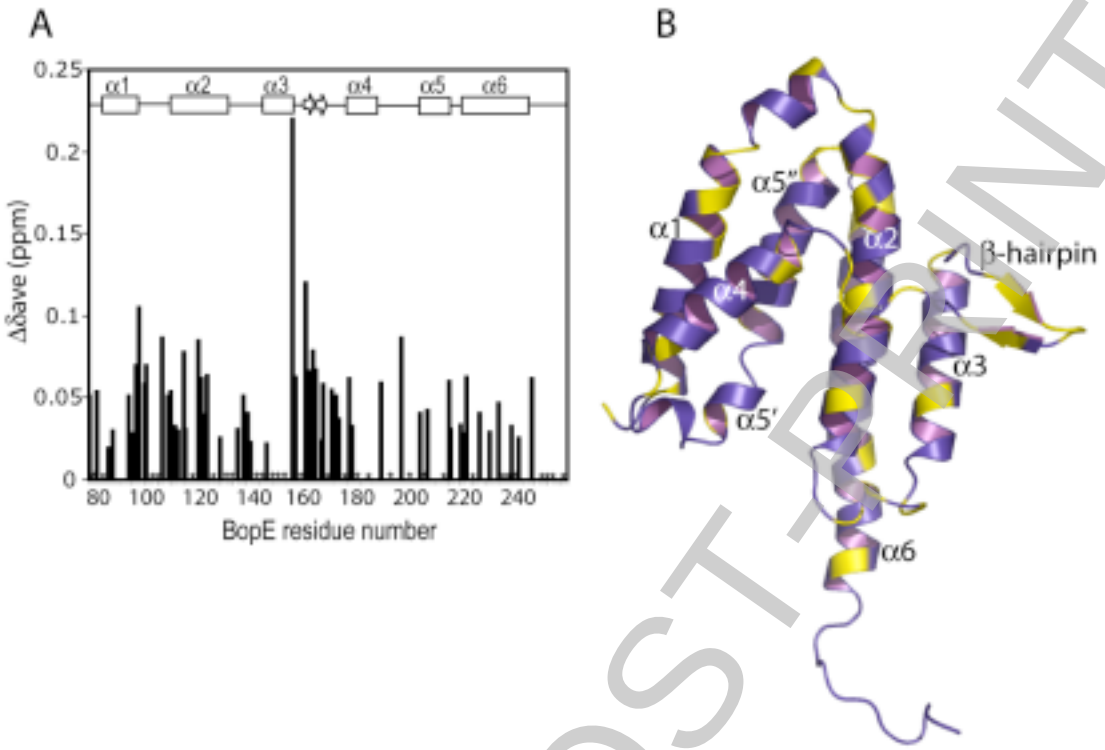

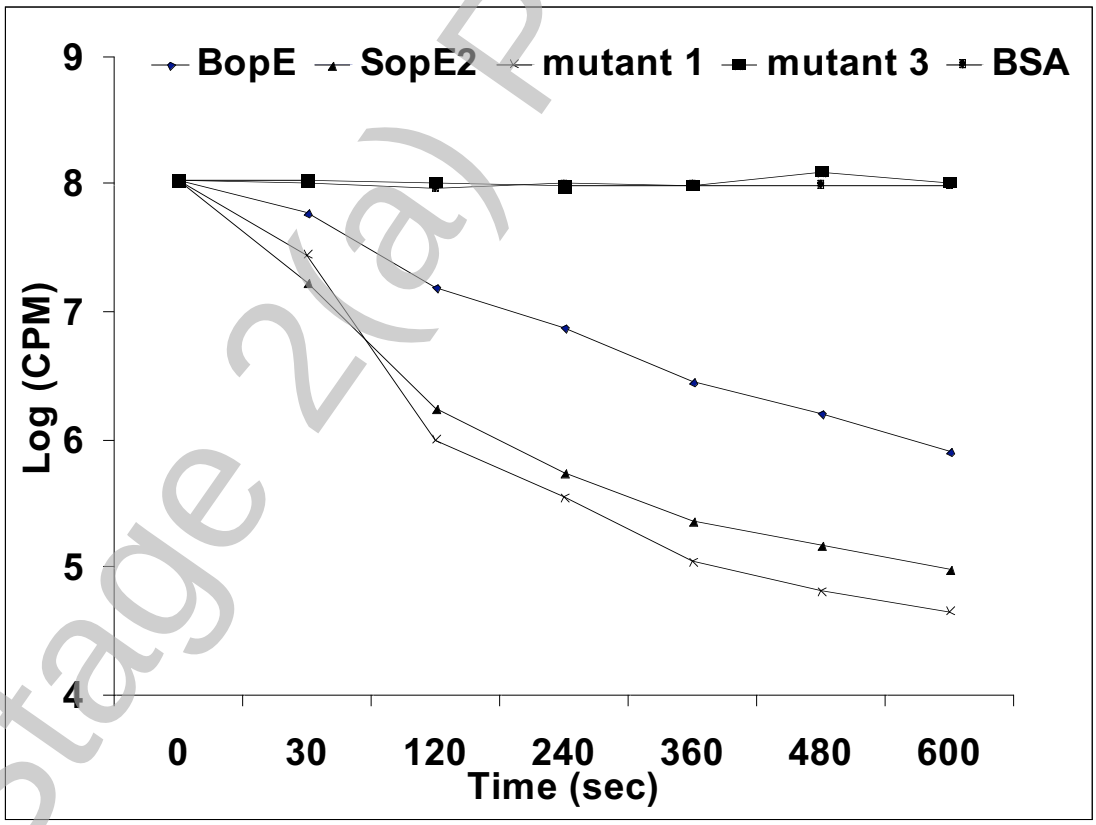

Figure 6